

Complex interplay of 3d and 4f magnetism in $\text{La}_{1-x}\text{Gd}_x\text{MnO}_3$

J. Hemberger¹, S. Lobina¹, H.-A. Krug von Nidda¹, N. Tristan¹,
V.Yu. Ivanov², A.A. Mukhin², A.M. Balbashov³, and A. Loidl¹

¹*Experimentalphysik V, Center for Electronic Correlations and Magnetism,
Institut für Physik, Universität Augsburg, D-86135 Augsburg, Germany*

²*General Physics Institute of the Russian Academy of Sciences, 38 Vavilov Street, 119991 Moscow, Russia*

³*Moscow Power Engineering Institute, 14 Krasnokasarmennaja Street, 111250 Moscow, Russia*

We report on structural, magnetic, electrical, and thermodynamic properties of Gd-doped LaMnO_3 single crystals for Gd doping levels $0 \leq x \leq 1$. At room temperature, for all doping levels the orthorhombic O' phase is indicative for a strong Jahn-Teller distortion. All compositions are insulating. The magnetism of $\text{La}_{1-x}\text{Gd}_x\text{MnO}_3$ is dominated by the relatively strong Mn-O-Mn superexchange. For increasing Gd doping the weakening of the nearest-neighbor exchange interactions due to the significant decrease of the Mn-O-Mn bond angles leads to the continuous suppression of the magnetic phase-transition temperature into the A-type antiferromagnetic low-temperature phase. The temperature dependence of the magnetization can only be explained assuming canting of the manganese spins. The magnetic moments of Gd are weakly antiferromagnetically coupled within the sublattice and are antiferromagnetically coupled to the Mn moments. For intermediate concentrations compensation points are found, below which the spontaneous magnetization becomes negative. In pure GdMnO_3 the Mn spins undergo a transition into a complex, probably incommensurate magnetic structure at 41.5 K, followed by a further ordering transition at 18-20 K revealing weak ferromagnetism due to canting and finally by the onset of magnetic order in the Gd sublattice at 6.5 K. At the lowest temperatures and low external fields both magnetic sublattices reveal a canted structure with antiparallel ferromagnetic components.

PACS numbers: 75.30.-m, 75.30.Hx, 77.30.Kz, 72.80.Ga

I. INTRODUCTION

Exactly since one decade, stimulated by the observation of colossal magnetoresistance effects by von Helmolt et al.¹ and Chahara et al.² the physics of doped manganese perovskites is in the focus of solid-state research. The enormous progress in this field is documented in recent review articles by Coey et al.,³ Nagaev,⁴ and Salomon and Jaime.⁵ In addition to their technological potential the manganites also represent an enormous and fascinating playground for basic solid-state research: unconventional and exotic ground states are established via the competing interplay of the internal degrees of freedom, like spin, orbital momentum, charge, as well as lattice degrees of freedom.⁶

In this communication we report on structural details, on susceptibility, magnetization and heat capacity of single crystalline $\text{La}_{1-x}\text{Gd}_x\text{MnO}_3$ and, hence, our focus is directed towards the isovalent doping of the A-site in RMnO_3 , with R denoting the rare-earth elements lanthanum ($4f^0$) or gadolinium ($4f^7$). From a general point of view, the rare-earth manganites can be grouped into two classes: the compounds from La to Dy (with the exception of Ce and Pm), characterized by larger ionic radii, reveal an orthorhombic perovskite-derived structure, while the compounds from Ho to Lu crystallize in a hexagonal structure, not related to the perovskites.⁷ Focusing on the first group, when going from La to Dy manganite, the tolerance factor decreases with the decrease of ionic radii and the buckling and tilting of the ideal cubic structure becomes stronger.⁸ Consequently the Mn-

O-Mn bond angles are reduced resulting in a strong suppression of the antiferromagnetic (AFM) ordering temperature of the Mn subsystem, from 140 K for LaMnO_3 to 40 K for TbMnO_3 and the corresponding transformation of the Mn magnetic structure from an antiferromagnetic layer A-type ordering with a weak ferromagnetism ($A_y F_z$) (La, Pr, Nd)⁷ to an incommensurate sinusoidal structure (Tb).⁹ At the same time, the Jahn-Teller (JT) transition, i.e. the orbital-order transition, which is well below 1000 K in LaMnO_3 , is shifted to values of almost 1500 K in TbMnO_3 .¹⁰ However, strong hysteresis effects, domain reorientation, history dependence, oxygen diffusion, and oxidation processes do not allow a precise determination of the JT transition temperatures.¹⁰

The magnetic moments of the rare-earth ions are polarized due to the coupling with the Mn subsystem resulting in a noticeable anisotropic contribution to the low-temperature magnetic and thermodynamic properties of the manganites as we have recently reported for PrMnO_3 and NdMnO_3 .¹¹ The coupling within the rare-earth sublattice is antiferromagnetic and rather weak. In many cases the rare-earth moments do not exhibit long-range magnetic order (and if, the ordering temperatures are below 10 K). The magnetic structure in the rare-earth manganites can be rather complex, as it has been recognized already long time ago. In TbMnO_3 Quezel et al.⁹ found a sine-wave ordering of the Mn^{3+} moments with the ordering wave vector along the b -axis below 40 K and a short-range incommensurate ordering of the Tb^{3+} moments with a different wave vector below 7 K. Similar magnetic structures were also observed in orthorhombic

HoMnO₃.^{12,13} Metamagnetic behavior has been detected in the Gd, Tb and Dy compounds.¹⁴

Turning now specifically to GdMnO₃, it has first been synthesized by Bertaut and Forrat¹⁵ and by Belov et al.¹⁶ The magnetic properties of pure GdMnO₃ were studied and have been reported previously by Troyanchuk et al.¹⁴ It was speculated that GdMnO₃ undergoes a smeared out phase transition into a complex magnetic order of the manganese sublattice below 40 K with the Gd sublattice antiferromagnetically ordered with respect to the Mn moments and that antiferromagnetic order within the Gd sublattice takes place below 6 K. In addition, a metamagnetic transition has been observed in external fields of 5 kOe.¹⁴ Based on susceptibility and Mössbauer results, Zukrowski et al.¹⁷ concluded that the Mn moments order at 40 K, while long-range magnetic order in the Gd sublattice is established below 20 K. Very recently several contributions concerning pure perovskitic rare earth manganites (containing pure LaMnO₃ and GdMnO₃) were published studying the interrelation between structural constraints and the magnetic and orbital structures. Both, Néel and orbital (JT) transition systematically depend on the in-plane Mn-O-Mn bond angle ϕ . The findings are interpreted in terms of spin frustration¹⁸ and orbital order-disorder transitions.¹⁹

In this work we provide a detailed study of the structural, magnetic and electrical properties of La_{1-x}Gd_xMnO₃. We use this system as a systematic variation of the Mn-O-Mn angle and relate it to the development of the complex magnetic groundstates. In addition, we provide heat-capacity results for GdMnO₃ as function of temperature and field to unravel the complex sequence of magnetic phase transitions in this compound and to derive a detailed (H, T)-phase diagram.

II. EXPERIMENTAL DETAILS

La_{1-x}Gd_xMnO₃ single crystals were grown in Ar flow by a floating-zone method with radiation heating for Gd concentrations $x = 0, 0.25, 0.5, 0.75$ and 1. X-ray powder-diffraction experiments were performed on powder of crushed single crystals at room temperature with a STOE diffractometer utilizing Cu-K α radiation with a wave length $\lambda = 0.1541$ nm. The magnetic susceptibility and the magnetization were recorded using a commercial SQUID magnetometer for temperatures $T < 400$ K and external magnetic fields up to 50 kOe. The electrical resistance has been measured using standard four-probe techniques in van-der-Pauw geometry²⁰ in home-built cryostats from 1.5 K to room temperature and in bar-type geometry in a home-built oven up to 1200 K. The specific heat was recorded in a home-built equipment using ac methods for temperatures $T < 200$ K and external magnetic fields up to 140 kOe.

The samples with $x = 1$ and 0.75 revealed a strong magnetic anisotropy with the easy direction of magnetization along the c -axis. The $x = 0.5$ and 0.25 samples

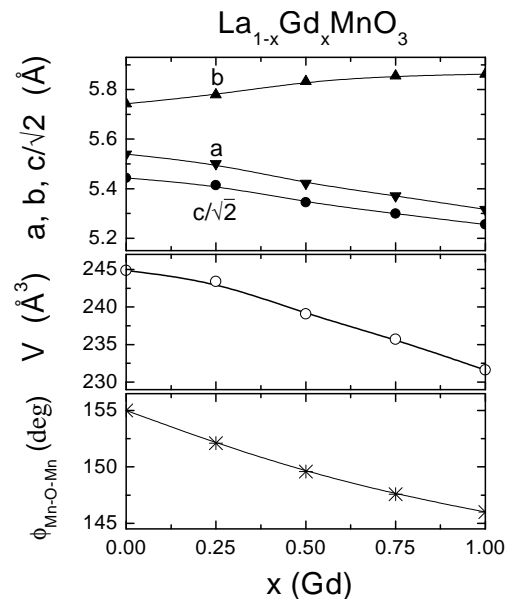


FIG. 1: Lattice constants a , b , and $c/\sqrt{2}$ (upper frame), volume of the unit cell (middle frame), and in-plane Mn-O-Mn bond angle ϕ in La_{1-x}Gd_xMnO₃ vs. Gd concentration x .

exhibited a weaker anisotropy probably due to the twin structure, resulting in an appearance of a spontaneous magnetization not only in the easy direction but also in a hard one. The data shown below, except a few ones for pure GdMnO₃, correspond to the measurements along the easy direction.

III. RESULTS AND DISCUSSION

From x-ray diffraction all samples investigated revealed the O' orthorhombic structure (Pbnm, JT distorted, see i.e. 21 for the canonical convention of the structural nomenclature). No impurity phases were detected above background level. The diffraction patterns were refined using Rietveld analysis. The lattice constants and the volume of the unit cell as derived from the profile analysis are shown in Fig. 1. For all concentrations we find $b > a > c/\sqrt{2}$ indicative for a static JT distortion superposed to the high temperature O-type (i.e. not JT distorted) orthorhombic structure which results from the buckling and tilting of the MnO₆ octahedra due to geometrical constraints. On increasing Gd concentration the lattice constants a and c are slightly decreasing, while b increases continuously. From this observation some remarkable structural details can be deduced: The parameter $\varepsilon = (b-a)/(a+b)$ characterizes the orthorhombic distortion. This distortion is continuously increasing on Gd doping due to the substitution of La ions by the smaller Gd. In addition, the increasing inequality of the lattice constants a and b with increasing x signals an increasing tilting of the octahedra around the b -axis and implies significant deviations of the Mn-O-Mn bond angle ϕ within

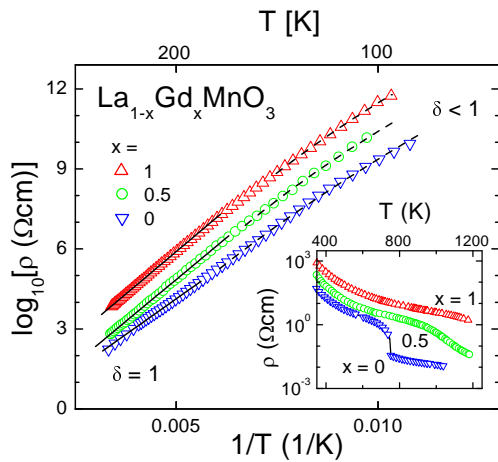


FIG. 2: Temperature dependence of the resistivity in $\text{La}_{1-x}\text{Gd}_x\text{MnO}_3$ for various compounds plotted in an Arrhenius representation. (The $x = 1$ curve is shifted for better clarity.) The solid lines at high temperatures represent Arrhenius fits indicating a purely activated type of behavior of the charge carriers. The dashed lines at low temperatures represent variable-range-hopping conductivity. Inset: Resistivity above 400 K.

th ab -plane from 180° . In the lowest frame of Fig. 1 we illustrate the concentration dependence of the in-plane Mn-O-Mn bond angle ϕ as estimated from the Rietveld refinement of the x-ray powder data.²² The G-type orbital order of LaMnO_3 determines the magnetic superexchange interactions between the Mn spins. The alteration of the orbital configuration via the Mn-O-Mn bond angle should influence in the magnetic properties of the spin system. According to the Kanamori-Goodenough rules (assuming 180° bond angles) the semi-covalent orientation of the e_g^1 orbitals within the ab -plane leads to ferromagnetic (FM) superexchange interactions, the covalent orientation of these orbitals along c -direction leads to AFM superexchange.²³ This results into the well known A-type AFM order with FM ab -planes coupled antiferromagnetically along the c -axis. The deviation of the in-plane Mn-O-Mn bond angles from 180° will weaken the FM interactions within the ab -planes but not alter the AFM coupling along c . The paramagnetic Curie-Weiss temperature θ is determined by the sum of FM in-plane interactions and AFM coupling along c . Concomitantly we expect a decrease of the Néel temperature for the manganese sublattice, determined by the sum of the absolute values of the different interactions.

The ratio $c/a < \sqrt{2}$ (see Fig. 1) almost remains constant. This indicates the absence of qualitative differences concerning the driving force of the JT distortion in all the compounds investigated. The reason is that the substitution of isovalent Gd^{3+} for La^{3+} gives Mn^{3+} in an octahedral environment for all Gd concentrations x , with one electron in the upper e_g doublet of the $3d$ manifold, which is JT active. As a consequence the transport properties do not change their insulating characteristics

for all Gd concentrations. Fig. 2 shows the resistivity for the pure compounds and for $x = 0.5$ in an Arrhenius representation. All samples show insulating behavior with a relatively high room-temperature resistivity of $\approx 3 \text{ k}\Omega\text{cm}$ (again demonstrating the good sample stoichiometry). At high temperatures the resistance of all samples can be described by a simple thermally activated behavior, indicated by straight solid lines in Fig. 2. The energy barriers are of the order of 0.2 to 0.25 eV, not systematically depending on concentration. At low temperatures significant deviations from an Arrhenius type of resistance behavior can be observed. In a temperature range below 150 K three-dimensional variable-range hopping following $\ln \rho \propto (T_0/T)^\delta$, with values of T_0 of the order of $5 \times 10^9 \text{ K}$ for $\delta = 1/4$, values typically observed in manganites.²⁴ It has to be stated that in the examined temperature range accessible below 150 K (limited by the upper value of the measurable impedance range) similar good fitting results can be achieved using an exponent of $1/2$ indicating the opening of a Coulomb gap and, therefore, no final conclusions on the influence of correlation effects on the hopping mechanisms can be drawn from this work.²⁵ However, from the resistivity results it seems that the electron-band structure is not altered significantly upon Gd doping. Hence, the JT ordering temperature is only influenced by the local lattice distortions of the oxygen octahedron due to geometrical constraints. And indeed, for pure LaMnO_3 the Jahn-Teller transition has been reported to occur at $T_{\text{JT}} = 750 \text{ K}$ ^{17,26}, while it is shifted to 950 K in pure PrMnO_3 .²⁷ The inset of Fig. 2 shows resistivity data for the pure compounds LaMnO_3 and GdMnO_3 and the mixed compound $\text{La}_{0.5}\text{Gd}_{0.5}\text{MnO}_3$ in a temperature range from 400 to 1200 K. In LaMnO_3 (triangles down) the JT transition can clearly be seen as a sharp jump in the resistivity curve. In GdMnO_3 no such feature can be detected demonstrating that the JT

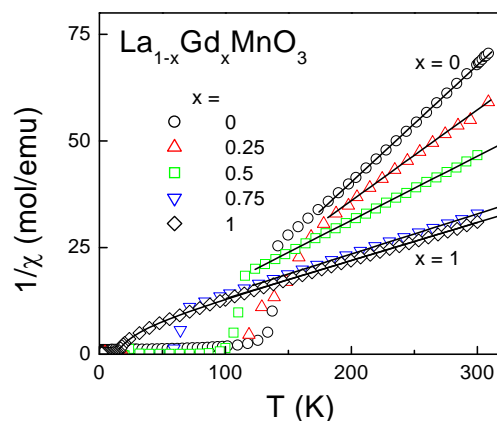


FIG. 3: Inverse dc susceptibility ($\chi = M/H$) versus temperature as measured in an external magnetic field of 10 Oe. The solid lines through the data for $x = 0, 0.25, 0.5$ and 0.75 represent fits to Curie-Weiss laws. The solid line through the data for $x = 1$ indicates the result of a fit taking into account two magnetic sublattices coupled ferrimagnetically.

transition occurs even above $T \approx 1200$ K. The increase of the JT transition temperature with decreasing Mn-O-Mn bond angle is in accordance with recent studies.^{18,19}

Fig. 3 shows the inverse magnetic susceptibilities for all concentrations investigated. At elevated temperatures all susceptibilities follow a Curie-Weiss (CW) law. The Curie constant is increasing due to the increasing contribution of the rare-earth moment (Gd^{3+} : spin-only, $S = 7/2$). As expected due to the decreasing bond angles (see Fig. 1) between neighboring Mn ions (Mn^{3+} : high-spin, $S = 2$) the Néel temperatures T_N are significantly decreasing. The dependence of T_N on the Mn-O-Mn bond angle fits well with the findings of Kimura et al.¹⁸ for other $R\text{MnO}_3$ compounds. As we will show in the following, with the exception of pure GdMnO_3 , no phase transition into a long-range AFM order of the Gd moments can be detected in the temperature range investigated. The concentration dependencies of the effective moments (lower frame), the CW temperatures θ (middle frame), and the magnetic transition temperatures (upper frame) are shown in Fig. 4. The onset of A-type AFM order at T_{CA} for the doped compounds is well indicated via the observation of a ferromagnetic component, due to spin canting (see later).²⁸ As stated above, T_{CA} continuously decreases from 140 K in LaMnO_3 to ≈ 20 K in GdMnO_3 . But in the pure Gd compound additional magnetic transitions into an incommensurate phase around $T_{IC} \approx 40$ K and into an AFM order of the Gd moments

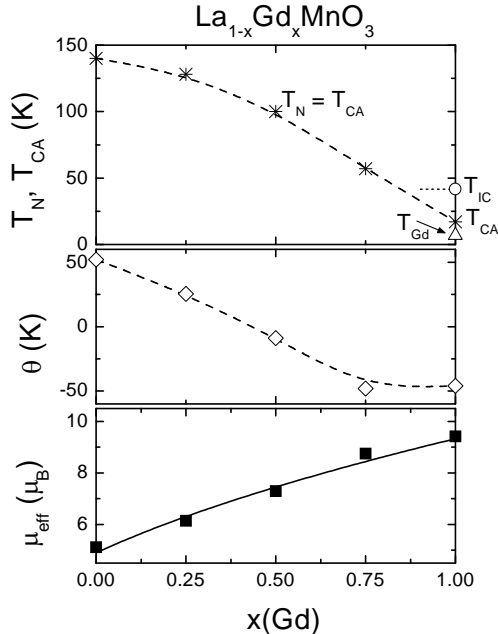


FIG. 4: Concentration dependencies of the parameters as obtained from the analysis of the susceptibility measurements: Néel temperatures (asterixes: upper frame), Curie-Weiss temperatures (open rhombs: middle frame), and paramagnetic moments (solid circles: lower frame). The solid line through the concentration dependence is a fit as described in the text. The dashed lines are drawn to guide the eye.

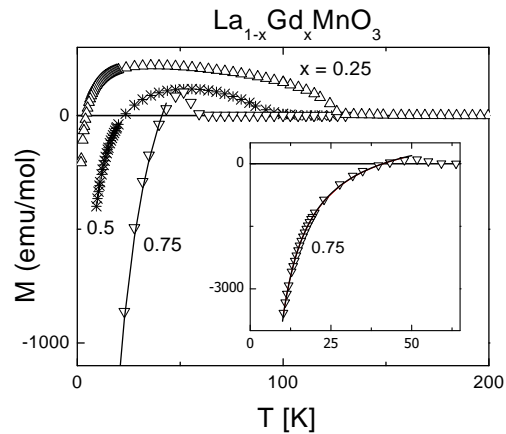


FIG. 5: Magnetization M vs. temperature in $\text{La}_{1-x}\text{Gd}_x\text{MnO}_3$ for $x = 0.25$ (triangles up), 0.5 (stars), and 0.75 (triangles down). The data were recorded on cooling from room temperature in an external magnetic field of 10 Oe. The solid line represents a fit which takes into account the paramagnetic contribution of the Gd subsystem polarized by the internal field of the manganese moments due to Gd-Mn coupling. Inset: Data and fit for $x = 0.75$ on an enlarged scale.

can be detected by dc- and ac-susceptibility measurements, as well as by heat-capacity experiments, which will be discussed later. The positive CW temperature θ of pure LaMnO_3 , which is an A-type antiferromagnet below 140 K, signals the importance of the ferromagnetic in-plane super-exchange interactions. θ continuously decreases with increasing Gd concentration. It is interesting to note that the CW temperatures become negative for Gd concentrations $x \geq 0.5$. This signals the decreasing importance of the ferromagnetic in-plane exchange on increasing x . As already discussed above the concentration dependent decrease of T_{CA} is related to the decreasing Mn-O-Mn bond-angles altering the orbital overlap. Obviously this effect influences particularly the FM superexchange interactions within the ab -plane, as already suggested in literature.¹⁹ The decreasing importance of the dominating ferromagnetic in-plane exchange enhances the influence of the AF next nearest-neighbor exchange in the ab -plane and promotes a change of the spin structure for the Mn sublattice, as will be discussed later for pure GdMnO_3 . However, the paramagnetic moments can well be approximated assuming $\mu_{eff}^2/(g\mu_B)^2 = x \times S_{Gd}(S_{Gd} + 1) + S_{Mn}(S_{Mn} + 1)$ (solid line in the lower frame of Fig. 4).

Fig. 5 provides a closer look on the magnetization of $\text{La}_{1-x}\text{Gd}_x\text{MnO}_3$ for concentrations $x = 0.25, 0.5$, and 0.75 as measured in fields of 10 Oe. At the magnetic ordering temperature we observe a spontaneous ferromagnetic moment which results from canting of the manganese spins. For the compounds with Gd concentrations $x = 0.25, 0.5$ and 0.75 we find clear indications for compensation points, the temperature of which increases on increasing x . Via the antiferromagnetic coupling of the Gd spins to the manganese moments, the

Gd spins are polarized antiparallel with respect to the FM component of the manganese spins, which can be explained by Dzyaloshinsky-Moriya interaction and is an intrinsic feature of the A-type AFM state in $RMnO_3$ systems.²⁸ With decreasing temperatures the Gd spins are more and more aligned in the exchange field of the manganese moments, following a Curie-type temperature dependence and finally yielding a negative magnetization at the lowest temperatures, when the polarization of the Gd spins exceeds the FM component of the Mn moments. The solid line in the inset of Fig. 5 shows that the negative magnetization M can well be approximated by $M = M_{Mn} + (H_{int} + H_{ext}) \times C_{Gd}/T$, where the spontaneous magnetization M_{Mn} and the internal field H_{int} result from the Mn moments and the external field is $H_{ext} = 10$ Oe. (Note that M_{Mn} was used as a fitting parameter and considered to be constant well below T_{CA} .) C_{Gd} is the Curie constant of the Gd moments. The best fit was obtained using an internal magnetic field of the order of 8 kOe created by the moments of the manganese sublattice.

Fig. 6 shows the magnetization $M(T)$ for $La_{0.5}Gd_{0.5}MnO_3$ in more detail for heating and cooling. The temperature cycles are indicated by arrows. Triangles down denote the cooling cycle in an external field of 10 Oe. At $T_N = 95$ K, the onset of a spontaneous magnetization along c indicates the appearance of a canted antiferromagnetic structure of the Mn moments. Compensation due to the AFM alignment of the Gd spins occurs close to 25 K. In the magnetization cycle, the magnetization now was switched to positive values by an external magnetic field of 50 kOe, the field was switched off again and then the sample was heated in a field of 10 Oe. As expected M is exactly reversed. The

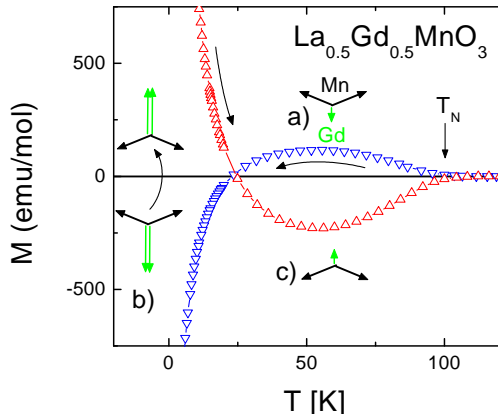


FIG. 6: Magnetization M vs. temperature for $La_{0.5}Gd_{0.5}MnO_3$ as measured in an external field of 10 Oe. The data were taken on cooling from room temperature (triangles down). At the lowest temperatures the magnetization was switched in an external field of 50 kOe. Then M was measured on heating (triangles up). The insets a), b), and c) indicate the spin structure at the respective temperatures and cycle positions.

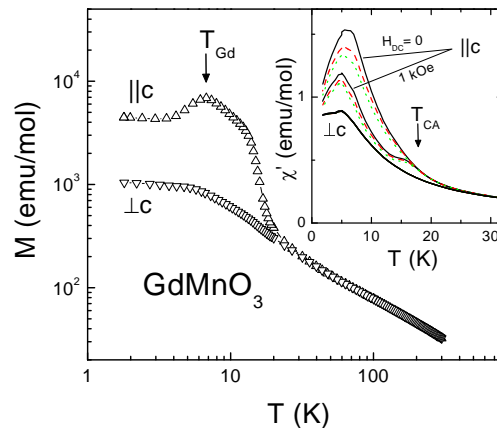


FIG. 7: Magnetization M vs. temperature for $GdMnO_3$ plotted on a double-logarithmic scale as measured in an external field of 1000 Oe. The easy (triangles up) and the hard direction (triangles down) are shown which split approximately at 20 K. The inset shows the ac susceptibility measured along c and within the ab -plane at a dc field of zero and 1000 Oe at 3 measuring frequencies of 1 (solid line), 35 (dashed line), and 1000 Hz (dotted line). Perpendicular to the c -axis no dependence on magnetic bias field or frequency can be detected.

spin structures in the ordered phases including the spin reversal are also indicated in Fig. 6.

Turning now to the magnetism of pure $GdMnO_3$, Fig. 7 shows magnetization vs. temperature on a double-logarithmic scale. Above 100 K the magnetization reveals the characteristics of a pure paramagnet and follows a Curie-Weiss law with a CW temperature $\theta = -35$ K. Down to 20 K the magnetization can well be described using a fit formula for the high-temperature susceptibility ($\chi = M/H$) taking both sublattices into account (see page 87 in Ref. 23) as shown as solid line in Fig. 3. Finally at $T_{CA} \approx 20$ K the magnetization reveals the onset of a significant anisotropy with a strong and abrupt increase in the easy direction (c -axis) due to the appearance of spontaneous magnetization in the canted state, while M only increases weaker and continuously along the hard direction ($\perp c$). A smeared-out peak indicates the onset of AFM long-range order of the Gd sublattice at $T_{Gd} \approx 7$ K. Corresponding results can be found in the ac susceptibility shown in the inset of Fig. 7. The anisotropic splitting of χ_{ac} parallel and perpendicular to the c -direction can clearly be observed. Below T_{CA} a weak frequency dependence for the susceptibility along c appears. In addition a shoulder at 18 K emerges in a magnetic bias field of 1 kOe. Both, field and bias dependence cannot be found perpendicular to the c -direction and can be explained by the dynamics of domains carrying a FM component in c -direction, present in the canted AFM state, and corresponding saturation effects. Towards lower temperatures a peak or kink follows at ≈ 7 K. Based on these susceptibility results one is tempted to deduce an ordering temperature of ≈ 20 K for the Mn and 7 K for the Gd

sublattice. But that the sequence of magnetic ordering transitions is even more complex will become clear from the heat-capacity measurements, which will be discussed later.

The complex magnetization of GdMnO_3 as a function of field is given in Fig. 8. An apparently paramagnetic magnetization behavior at 30 K (we will see later that at 30 K GdMnO_3 has to be characterized as an antiferromagnet with the hysteresis shifted to higher fields), is followed at 24 K by a $M(H)$ behavior, with the typical signature of a metamagnetic phase transition at 20 kOe. On decreasing temperatures this metamagnetic transition shifts towards lower fields and bears the characteristics of a weak ferromagnet at 9 K. At the lowest temperatures, below the ordering temperature of the Gd sublattice, a complex hysteresis loop develops with a remnant magnetization which however remains small and is well below $1 \mu_B$ even at 1.8 K. This complex hysteresis and the small remnant magnetization signal show that at low fields ($H < 5$ kOe) and low temperatures ($T < 6$ K) both sublattices are canted and the ferromagnetic components of the two sublattices are antiparallel to each other. As the magnetization always increases with increasing field to values well above the value of the ordered moment of Mn^{3+} , we believe that the FM component of the Gd spins points in the direction of the external field. At 50 kOe the magnetization of GdMnO_3 reaches values slightly above $5 \mu_B$, hence the manganese moments remain canted reducing the ordered moment of Gd from $7 \mu_B$ to almost $5 \mu_B$. No indications for a further spin reorientation (such as e.g. a spin-flop transition of the Mn spins) and no increase of the magnetization above $M = 6 \mu_B/\text{f.u.}$ can be detected in fields up to 140 kOe at $T = 5$ K (not shown).

Fig. 9 presents the results of the heat-capacity measurements in GdMnO_3 as function of temperature and field. The heat capacity, plotted as C/T , is shown for

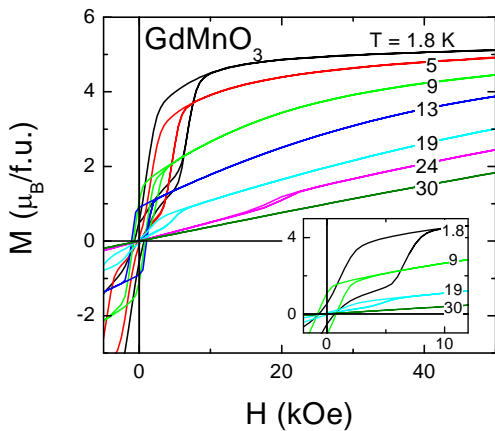


FIG. 8: Magnetization along c as function of the external magnetic field for a series of temperatures between 1.8 K and 30 K. The inset shows the hysteresis loops at low fields on an enlarged scale.

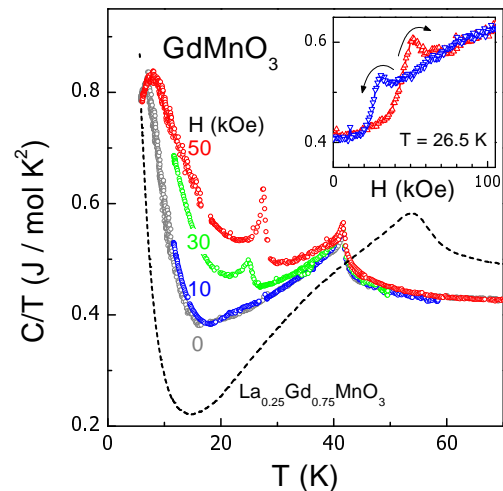


FIG. 9: Heat capacity of GdMnO_3 plotted as C/T as a function of temperature, measured at different external magnetic fields up to 50 kOe. The dashed line represents data for $\text{La}_{0.25}\text{Gd}_{0.75}\text{MnO}_3$ in zero external field. The inset shows the field dependence of the heat capacity of GdMnO_3 at $T = 26.5$ K.

temperatures $T < 70$ K, in external magnetic fields up to 50 kOe. A well defined heat-capacity anomaly, almost independent of the external field, shows up close to 40 K. It has to be noted that at this temperature no anomaly can be found in magnetic susceptibility measurements. From this it becomes clear that this anomaly does not result from the transition into the canted A-type AFM phase but has to be interpreted as onset of an incommensurate AFM spin structure¹⁸, which gives no macroscopic FM moment. A further broad peak with a cusp-like anomaly appears at 7 K. On increasing magnetic fields this low-temperature anomaly is shifted slightly to higher temperatures and is smeared out gaining a much higher weight of entropy between 7 and 40 K on increasing fields. This Schottky-type contribution obviously results from the alignment of the Gd spins within the external field amplified by the effective field of the canted Mn-spin structure setting in at $T_{\text{CA}} \approx 20$ K, as known from the susceptibility measurements. In fields of 30 kOe and 50 kOe a further anomaly shows up close to 25 K, which is strongly dependent on the external field. It probably corresponds to the metamagnetic transition into a canted antiferromagnetic state visible in $M(H)$ in an external field (e.g. at 20 kOe and a temperature of 24 K, as displayed in Fig. 8). Presumably it merges with the Gd anomaly at lower temperatures at lower fields (on the other hand we cannot exclude a strong reduction of this anomaly with decreasing magnetic field), corresponding to the observation that the hysteresis loops are shifted to low magnetic fields at low temperatures (Fig. 8). For comparison the dashed line in Fig. 9 exhibits the C/T data for the composition $\text{La}_{0.25}\text{Gd}_{0.75}\text{MnO}_3$. Here the above described complex findings are different. At $T_{\text{N}} = T_{\text{CA}} \approx 55$ K a cusp-like anomaly can be found which corresponds to

the transition into the canted AFM state (see Fig. 4). A shoulder in the displayed temperature dependence of C/T below T_{CA} and the strong increase towards low temperatures denote the polarization of the Gd spins within the effective field of the Mn sublattice. But no evidence for a further magnetic transition of the Mn sublattice into an incommensurate phase was found.

From the ac- and dc-susceptibility measurements, the magnetization, and the heat capacity we can construct a detailed (H, T) -phase diagram which is shown in Fig. 10. The paramagnetic regime of both sublattices above 40 K, is probably followed by an incommensurate sinusoidal (or spiral) structure of the manganese moments (in analogy to results for $TbMnO_3$ ⁹ and $o\text{-}HoMnO_3$ ¹²) and an almost paramagnetic gadolinium sublattice. Macroscopically any FM component of the sinusoidal Mn order is averaged out. This means that there is also no macroscopic net polarization of the Gd sites induced by the sinusoidal structure of the manganese spins. Towards lower temperatures this phase is followed by a canted structure of the manganese moments exhibiting a small FM component, due to which the Gd spins are polarized antiferromagnetically. The FM contribution of the Gd spins is larger than the FM contribution of the canted AFM state of the Mn spins, directing the Gd moments parallel to the external field. Only for sufficiently low temperatures and external magnetic fields the Gd sublattice itself can setup an additional antiferromagnetic (Gd-Gd) ordering, and we find a canted structure for both Gd and Mn sublattices, still antiferromagnetically coupled. For higher external magnetic fields this state is suppressed.

IV. CONCLUSION

We have presented a detailed study on single crystals of $La_{1-x}Gd_xMnO_3$ covering the complete concentration range including pure $GdMnO_3$. Structural, magnetic,

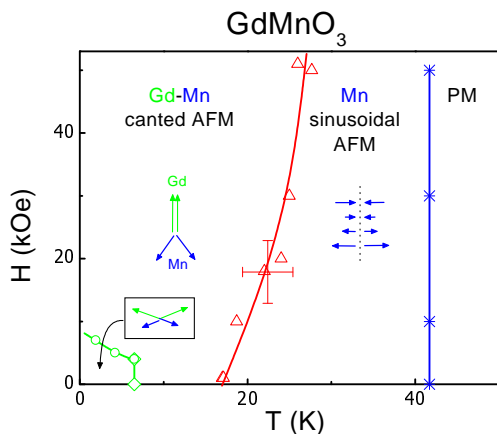


FIG. 10: (H, T) -phase diagram of $GdMnO_3$. The spin structures of the two magnetic sublattices are indicated.

electrical, and thermodynamic properties have been reported. The concentration dependence of the lattice constants signals the increase of orthorhombicity via a stronger tilting and buckling. This results from the decrease of the tolerance factor via the substitution of the larger La by the smaller Gd ions. The overlaying JT distortion and corresponding orbital order does not seem to be changed considerably. At low temperatures the electronic charge transport is dominated by hopping processes indicative for a disordered semiconductor with a finite density of localized states. At elevated temperatures all samples reveal a purely thermally activated charge transport. The temperature of the JT transition in $GdMnO_3$ could be estimated in the present work to be higher than 1200 K. From the susceptibility and magnetization measurements of the doped compounds we provide clear experimental evidence for a ferromagnetic contribution of the magnetic order of the manganese moments and for magnetic compensation due to the increasing influence of the Gd moments which are antiferromagnetically aligned in the internal field of the Mn moments. The experimental observation of magnetic compensation and spin reversal clearly indicates the importance of spin canting of the manganese moments. Since the doping is isovalent, double-exchange interactions cannot play any role and spin canting probably results from the Dzyaloshinsky-Moriya interaction.²⁸ This canted A-type AFM spin state persists for low temperatures within the whole concentration range.

Finally, for pure $GdMnO_3$ we observe a magnetic phase transition at 40 K. We argue that below 40 K the manganese moments develop a sinusoidal or another complex spin order. No polarization occurs at the Gd site and the Gd spins behave paramagnetically. Below 16-20 K spin canting of the manganese moments occurs, polarizing the Gd $4f$ spins, and for further decreasing temperatures a weak ferromagnetic moment evolves. Finally, at 6.5 K due to the interaction of the $4f$ spins, long-range order of the Gd moments evolves, yielding a canting of the Gd spins with a FM component antiparallel to the FM moment of the canted manganese spins. In finite external fields this state is suppressed: the canting angle of the Gd-spins is reduced yielding the full Gd moment in direction of the external field (reduced by the FM moment of the canted Mn-lattice).

Acknowledgments

This work was partly supported by the Bundesministerium für Bildung und Forschung (BMBF) via Grant No. VDI/EKM 13N6917-A, by the Deutsche Forschungsgemeinschaft via Sonderforschungsbereich SFB 484 (Augsburg), and by INTAS and Russian Foundation for Basic Researches N 03-02-16759.

-
- ¹ R. von Helmolt, J. Wecker, B. Holzapfel, L. Schultz, and K. Samwer, *Phys. Rev. Lett.* **71**, 2331 (1993).
- ² K. Chahara, T. Ohono, M. Kasai, Y. Kanke, and Y. Kozono, *Appl. Phys. Lett.* **62**, 780 (1993).
- ³ J.M. Coey, M. Viret, and S. von Molnar, *Adv. Phys.* **48**, 167 (1999).
- ⁴ E.L. Nagaev, *Physics Reports* **346**, 387 (2001).
- ⁵ M.B. Salomon and M. Jaime, *Rev. Mod. Phys.* **73**, 583 (2001).
- ⁶ Y. Tomioka, A. Asamitsu, H. Kuwahara, and Y. Tokura, in "Physics of the Manganites", (T.A. Kaplan, S.D. Mahanti, eds.), Kluwer Academics/Plenum Publisher, New York, 1998, p. 155.
- ⁷ R. Pauthenet and C. Veyret, *J. de Physique* **31**, 65 (1970).
- ⁸ M. Imada, A. Fujimori, and Y. Tokura, *Rev. Mod. Phys.* **70**, 1039 (1998).
- ⁹ S. Quezel, F. Tcheou, J. Rossat-Mignod, G. Quezel, and E. Roudaut, *Physica B* **86-88**, 916 (1977).
- ¹⁰ I.A. Troyanchuk, A.I. Akimov, G.I. Savchuk, and N.V. Kaspar, *Crystallographic Reports* **39**, 971 (1994).
- ¹¹ J. Hemberger, M. Brando, R. Wehn, V.Yu. Ivanov, A.A. Mukhin, A.M. Balbashov, and A. Loidl, *Phys. Rev. B*, to be published; cond-mat/0311170.
- ¹² H.W. Brinks, J. Rodriguez-Carvajal, H. Fjellvag, A. Kjekshus, and B.C. Hauback, *Phys. Rev. B* **63**, 094411 (2001).
- ¹³ A. Munoz, M.T. Casais, J.A. Alonso, M.J. Martinez-Lope, J.L. Martinez, and M.T. Fernandez-Diaz, *Inorg. Chem.* **40**, 1020 (2001).
- ¹⁴ I.A. Troyanchuk, N.V. Kaspar, H. Szymczak, and A. Nabalak, *Low. Temp. Phys.* **23**, 300 (1997).
- ¹⁵ F. Bertaut and F. Forrat, *J. de Physique* **17**, 129 (1956).
- ¹⁶ K.P. Belov, M.A. Zaitseva, and A.V. Ped'ko, *JETP* **36**, 1672 (1959).
- ¹⁷ J. Zukrowski, M. Wasniowska, Z. Tarnawski, J. Przewoznik, J. Chmista, A. Kozłowski, and K. Krop, *Acta Physica Polonica B* **34**, 1533 (2003).
- ¹⁸ T. Kimura, S. Ishihara, H. Shintani, T. Arima, K.T. Takahashi, K. Ishizaka, and Y. Tokura, *Phys. Rev. B* **68**, 060403 (2003).
- ¹⁹ J.-S. Zhou and J.B. Goodenough, *Phys. Rev. B* **68**, 054403 and 144406 (2003).
- ²⁰ L.J. van der Pauw, *Philips Research Reports* **13**, 1 (1957).
- ²¹ J.B. Goodenough and J.M. Longo, *Landolt-Börnstein: New Series III 4a*, Berlin 1970, p. 126.
- ²² Even though the x-ray powder diffraction measurements cannot reveal reliable oxygen positions, the Mn-O-Mn bond angles could be estimated assuming a linear relation to the y -parameter of the Gd sites (tilting distortion along b). The absolute values for the bond angles (within the ab -plane) were scaled on literature results¹⁸ for the pure compounds LaMnO₃ and GdMnO₃.
- ²³ J.B. Goodenough, "Magnetism and the chemical bond", Interscience publishers, New York, 1963.
- ²⁴ M. Paraskevopoulos, F. Mayr, J. Hemberger, A. Loidl, R. Heichele, D. Maurer, V. Müller, A.A. Mukhin, and A.M. Balbashov, *J. Phys.: Cond. Mat.* **12**, 3993 (2000).
- ²⁵ A. Seeger, P. Lunkenheimer, J. Hemberger, A.A. Mukhin, V.Yu. Ivanov, A.M. Balbashov, and A. Loidl *J. Phys.: Cond. Mat.* **11**, 3273 (1999).
- ²⁶ A.A. Mukhin, V.Yu. Ivanov, V.D. Travkin, S.P. Lebedev, A. Pimenov, and A. Loidl, and A.M. Balbashov, *JETP Letters* **68**, 356 (1998).
- ²⁷ Z. Jirak, S. Krupicka, Z. Simsa, M. Dlouha, and S. Vratislav, *J. Magn. Magn. Mater.* **53**, 153 (1985).
- ²⁸ I. Solovyev, N. Hamada, and K. Terakura, *Phys. Rev. Lett.* **76**, 4825 (1996); V. Skumryev, F. Ott, J.M.D. Coey, A. Anane, J.-P. Renard, L. Pinsard-Gaudart, and A. Revcolevschi, *Eur. Phys. B* **11**, 401 (1999).